An Integrated Friction Model Structure with Improved Presliding Behavior for Accurate Friction Compensation

Jan Swevers, Farid Al-Bender, Chris G. Ganseman, and Tutuko Prajogo

***Abstract*—This paper presents a new dynamical friction model structure which allows accurate modeling both in the sliding and the presliding regimes. Transition between these two regimes is accomplished without a switching function. The model incorporates a hysteresis function with nonlocal memory and arbitrary transition curves. These last aspects prove essential for modeling presliding friction that is encountered in real physical situations. The model as a whole can also handle the Stribeck effect and stick-slip behavior as has been demonstrated by validation on a KUKA IR 361 robot. In this sense, this model can be considered as more complete in comparison with others found in the literature. The general friction model allows modeling of individual friction systems through the identification of a set of parameters that determine the complete behavior of the system. In this way, the model structure has been used to identify the friction behavior of a linear slide as well as that of the above mentioned KUKA robot. The results of the latter identification have been consequently used for feedforward friction compensation to obtain the most accurate tracking.**

***Index Terms*—Friction, mechatronics, motion control, nonlinear systems.**

I. Introduction

FRICTION in mechanical systems is a nonlinear phenomenon that has many diverse aspects giving rise to control problems such as static errors, limit cycles, and stick-slip. Controllers that usually consider only the linear and the Coulomb parts of friction, and thus regarding the other aspects as disturbances, may yield unsatisfactory results if very accurate control, e.g., at velocity reversal, is required.

Friction is a result of extremely complex interactions between the surface and the near-surface regions of the two interacting materials as well as other substances present such as lubricants. Thus, accurate quantitative predictions of friction, based on surface and lubricant properties, are not yet possible [5]. However, the conceptual quantitative understanding of friction processes is now quite advanced so that macroscopically observed friction phenomena can be explained and used to derive analytical models.

The friction modeling considered here aims at the construction of a more comprehensive friction prediction model that accounts for the various aspects of that phenomenon so that mechanical systems with friction can be more accurately identified and consequently better controlled.

In building up an elaborate friction model structure, one begins by distinguishing two different friction regimes.

1) The so-called presliding regime or the micro-slip regime in which the adhesive forces (at asperity contacts) are dominant such that the friction force appears to be a function of displacement rather than the velocity. This is so because asperity junctions deform elasto-plastically (depending on their individual loading) thus behaving like nonlinear springs. As the displacement increases more and more junctions will break resulting eventually in gross sliding (second regime below). This "break-away" displacement may depend on diverse characteristics of the contact and surface texture: topography, hardness, surface layer metallurgy, etc. Armstrong [4], for example, reports 2–5 μm in steel junctions, which due to motion amplification (gears, lever arms) may, however, result in movements on the order of millimeters in other parts of a mechanism, e.g., in robots. Alternatively, microslip can be viewed as resulting from asperity contacts with a given random distribution each of which obeying Coulomb friction laws [6].
2) The so-called gross sliding regime in which all asperity junctions have broken apart (alternatively, all asperity contacts) such that the friction force is now a more pronounced function of sliding velocity, due for example to the build up of lubricating films.

The transition between these two regimes must not be considered as a sudden discontinuity in the sliding process, since there is a build up in micro-slip leading to gross-slip.

In a subsequent step the model is complemented by the addition of the dynamical aspects of the process.

The classical description of friction in the sliding regime is a static relation between velocity and friction force, the simplest of which consists of a superposition of Coulomb and viscous friction. A more elaborate model considers the Stribeck effect yielding a better approximation at low velocities [3], but in either case the friction force experiences a step jump at the origin, i.e., the presliding regime is not accounted for. On the other hand, some researchers, [10], [12], being preoccupied with small amplitude sliding and rolling, have considered presliding behavior alone, and thereby described the nature of frictional behavior in the quasistatic presliding regime. In a later stage, some researchers, e.g., Hess *et al.* [15], have shown experimen-

Manuscript received January 7, 1998; revised October 30, 1998 and March 30, 1999. Recommended by Associate Editor, Bastin.

The authors are with the Mechanical Engineering Department, Katholieke Universiteit Leuven, Celestijnenlaan 300 B, B3001 Heverlee, Belgium (e-mail: Jan.Swevers@mech.kuleuven.ac.be).

Publisher Item Identifier S 0018-9286(00)03238-4.

tally that sliding friction possess a dynamics, e.g., there is a time lag between velocity and friction force.

Armstrong *et al.* [4] have analyzed all these model aspects in order to derive a general model structure which includes a switching function between the two friction regimes. Such a switching is physically not justified and results in insurmountable obstacles in implementation [14]. In order to overcome these shortcomings, Canudas de Wit *et al.* [9] reformulated the model so that no switching function is needed while retaining all the other above mentioned aspects of friction. Their model, called the *LuGre model*,[1] resembles the Dahl model in the presliding regime, but in addition it allows arbitrary constant-velocity characteristics, e.g., the Stribeck effect, in the sliding regime. Friction in sliding and presliding are described by one differential equation and one output equation. While being very elegant and easy to implement, this model appears to oversimplify the actually observed frictional behavior. Armstrong [2] noted, for example, that the LuGre model has not been shown to accurately predict the friction observed in any apparatus, and that, furthermore, there are less degrees of freedom available than the number of physically distinct phenomena to be modeled. In our opinion, the shortcoming of this model lies in the inadequacy of the hysteresis part since: 1) it does not account for nonlocal memory [18] and 2) it cannot accommodate arbitrary displacement-force transition curves. A hysteresis behavior with nonlocal memory is defined as an input–output relationship for which the output at any time instant not only depends on the output at some time instant in the past and the input since then, but also on past extremum values of the input or output as well [18].

This paper proposes a model that includes all the various aspects mentioned above while overcoming the shortcomings of the LuGre model, verifies its essential aspects experimentally, and uses friction identification results successfully in accurate control.

Section II describes the LuGre model in more detail and points out its shortcomings. Section III describes the proposed dynamic friction model that includes a hysteresis model with nonlocal memory and arbitrary displacement-force transition curves. Section IV describes the estimation of the friction model parameters for the first axis of an industrial robot. Section V describes the behavior of the model and shows that it corresponds to known friction characteristics and those of the robot. Section VI describes two applications of the developed friction modeling: the identification of the low velocity friction behavior of a linear slide and the accurate tracking at very low speeds of the first joint of the above-mentioned robot using friction feedforward based on an identified friction model.

II. The LuGre Model

Canudas de Wit *et al.* [9] combine the Dahl model with arbitrary steady-state friction characteristics which can include the Stribeck effect. The model contains a state variable representing the average deflection of elastic bristles which are a visualization of the topography of the contacting surfaces. The resulting model shows most of the known friction behavior like presliding displacement, frictional lag, varying break-away force and stick-slip motion, and has already been used for friction compensation in a hydraulic servo system [11] and on the vertical axis of an electro-discharge machine [1]. However, hysteretic behavior with nonlocal memory between displacement and applied force in presliding as measured in [12] and [22] on different types of contact cannot be accounted for by this model. This may result in an overestimation of the energy dissipation in the presliding regime as will be shown further in this text.

[1]From a personal communication with Canudas de Wit.

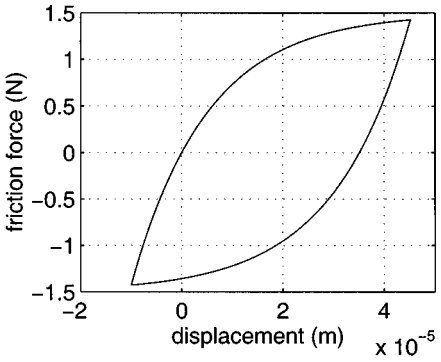

Fig. 1. LuGre model presliding simulation results obtained when the external force is ramped up and down between a negative and positive value with equal magnitude, starting from zero initial conditions.

The LuGre model consists of a nonlinear state, (1) below, and a friction force (output) (2)

$$\frac{dz}{dt} = v - \frac{|v|}{g(v)}\, z \tag{1}$$

$$F = \sigma_0 z + \sigma_1 \frac{dz}{dt} + \sigma_2 v \tag{2}$$

with z the state variable, v the velocity ($=dx/dt$), $g(v)$ a function that models the constant velocity behavior, σ_0 an equivalent stiffness for the position-force relationship at velocity reversal, σ_1 the micro-viscous friction coefficient, and σ_2 the viscous friction coefficient.

Whereas the model allows a good description of the constant velocity behavior and offers a smooth transition at velocity reversal, the modeling capabilities in presliding regime are restricted as follows.

- The model is too dissipative in presliding.
- The shape of the transition curve is fixed by the model structure and therefore cannot be adapted to actually measured values.

Both modeling problems are discussed below.

Neither the Dahl nor the LuGre model make any attempt to include hysteresis with nonlocal memory. Both models show a hysteresis-like behavior only when the extreme points lie symmetrically with respect to the origin (Fig. 1), which does not agree with experimentally observed behavior as described in [12] and [23].

Fig. 2 shows other simulation results obtained with the LuGre model (simulation model and parameter values are taken from [9]). In the simulation, the driving force f is ramped up from A to B, then ramped down from B to C and then ramped up again from C to D. The displacement-force relation that is obtained does not correspond with experimentally observed friction char-

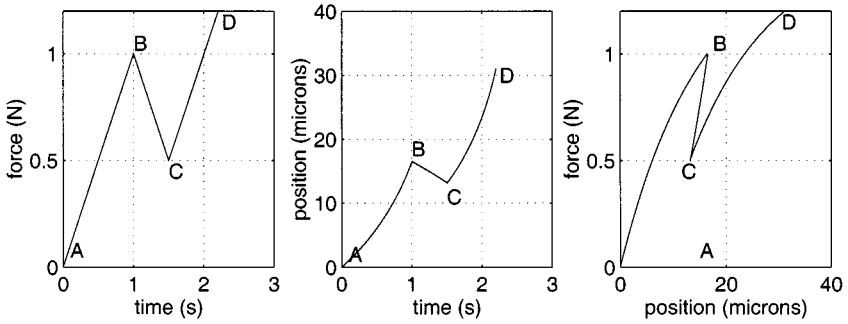

(a) (b) (c)

Fig. 2. LuGre model presliding simulation results: (a) applied external force, (b) resulting position, and (c) resulting position-force relation.

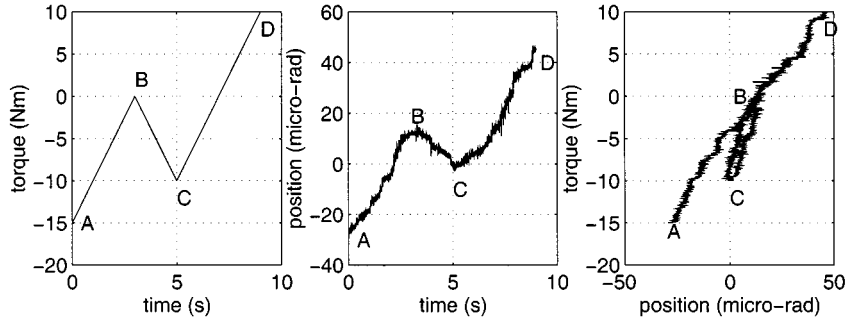

(a) (b) (c)

Fig. 3. Presliding measurements on the first axis of a KUKA 361 IR robot using a eddy-current proximity sensor: (a) applied torque, (b) measured angular position, and (c) resulting position-torque relation.

acteristics [12]. Fig. 3 shows presliding friction torque measurements on the first joint of an industrial KUKA IR 361. During the experiment, the applied force was ramped up and down just like in the simulation. The friction curve in Fig. 2 is clearly different from the curve in Fig. 3, which includes a closed part that has also been reported in [12]: the measured curve closes when the applied torque is ramped up from C to D and the friction force returns to the initial transition curve. This is typical of hysteresis with nonlocal memory [18]. Moreover, the energy dissipation, which is equal to the net area under this displacement-friction force (torque) curve, is much larger in the LuGre model and so is the resulting displacement.

The position-force relationship in presliding is implicitly defined by the two model equations. The nonlinear state (1) defines an implicit relationship between dz/dt and dx/dt and consequently between z and x. Equation (2) defines a relationship between F and z as the damping contributions $(\sigma_1(dz/dt) + \sigma_2(dx/dt))$ in presliding are normally negligible. The model thus defines an implicit relationship between x (or equivalently relative displacement) and the friction force F. Beside the parameter σ_0 which models the initial stiffness at velocity reversal, no parameters are left for the shaping of the transition curves which will then always have the same form as depicted in Fig. 1. The LuGre model is therefore inadequate for fitting transition curves of arbitrary forms.

Fig. 4 shows a typical instance of this. The parameter σ_0 has been fitted such that the prediction error is minimized in a least squares sense. The model cannot capture the high initial stiffness accuring immediately after the velocity reversal.

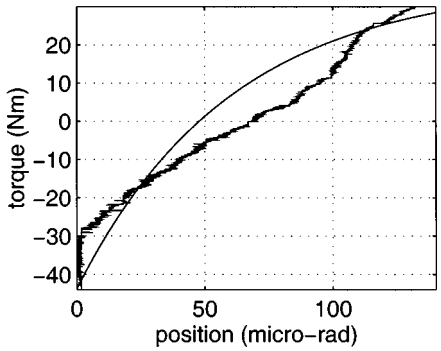

Fig. 4. Comparison of transition curve predicted by the LuGre model and transition curve measured on the first axis of a KUKA IR 361 robot using an eddy-current proximity sensor.

III. A Novel Friction Model

The friction force F is modeled by a set of two equations which, as is the case of the LuGre model, depend on a state variable z representing the average deformation of the asperities of the contacting surfaces.

1) The *friction force equation* yields the friction force based on the current hysteresis transition curve, the derivative of the state variable z, and the current velocity

$$F = F_h(z) + \sigma_1 \frac{dz}{dt} + \sigma_2 v \tag{3}$$

where σ_1 where is a micro-viscous damping coefficient, σ_2 is the viscous damping coefficient, and v is the ve-

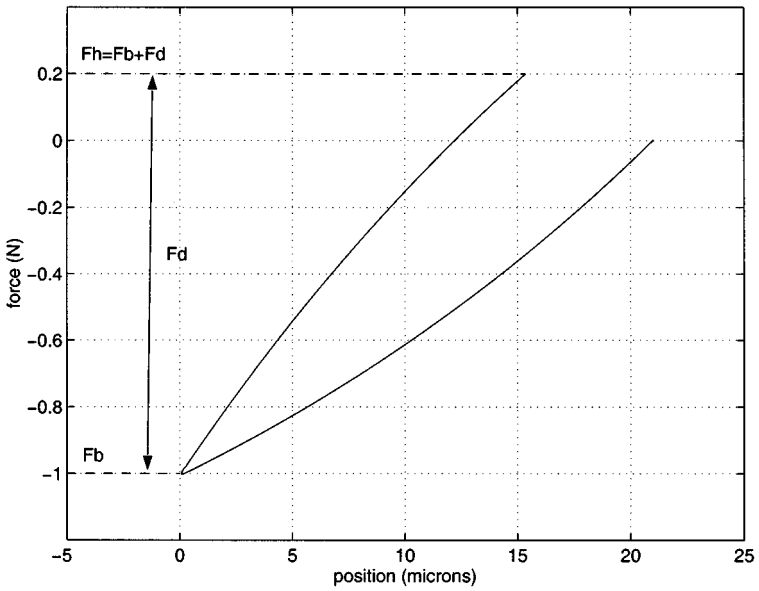

Fig. 5. F_b and F_d on the current hysteresis transition curve.

locity of the moving object. $F_h(z)$ is the hysteresis friction force, i.e., the part of the friction force exhibiting hysteretic behavior. It is a static hysteresis nonlinearity with nonlocal memory [3]. That is to say that it is a multibranch nonlinear function for which:

a) branch-to-branch transitions occur after velocity reversals;
b) the branches (transition curves) are determined only by the past extremum values of F_h, i.e., are independent of the particular manner of the variation of z between extremum points;
c) the future values of F_h past any time instant t_0 not only depend on the value of F_h at t_0 and the values of z at all subsequent instants of time $t \geq t_0$, but also on past extremum values of F_h.

This last property is in contrast to the behavior of hysteresis nonlinearities with *local* memory, where the past exerts its influence upon the future through the current value of the output only [18].

This part of the friction is modeled by a hysteresis function $F_h(z)$ consisting of transition curves (curves between two reversal points or extrema). Each velocity reversal initiates a new transition curve, adds a new extremum to the hysteresis memory, and resets the state variable z to zero. The transition curve which is active at a certain time will be called the current transition curve and is represented by $F_d(z)$. The value of $F_h(z)$ at the beginning of a transition curve is represented by F_b (see Fig. 5)

$$F_h(z) = F_b + F_d(z). \tag{4}$$

F_d is a point-symmetrical strictly increasing function of z, e.g., a piecewise-linear spring characteristic [12]. This function can be obtained from experimental identification as discussed below. On the other hand, it can be obtained from purely theoretical modeling of asperity contacts which are assumed to have a certain random distribution [6]. Sections III-A, III-B, and V give a more detailed description of the hysteresis model, its implementation, and properties.

2) The *nonlinear state equation* is based on the current hysteresis transition curve and the current velocity

$$\frac{dz}{dt} = v\left(1 - \text{sign}\left(\frac{F_d(z)}{S(v) - F_b}\right) * \left|\frac{F_d(z)}{S(v) - F_b}\right|^n\right). \tag{5}$$

$S(v)$ models the constant velocity behavior in sliding. The parameter n is similar to the exponent found in the general Dahl model [10]. It allows us to modify the influence of $F_d(z)/(S(v) - F_b)$ on the difference between dz/dt and v, such that the model behavior correspond better to friction measurements in the transition from presliding to sliding. For example, for high positive values of n, dz/dt will be different from v only when $F_d(z)$ is close to $S(v) - F_b$.

The following sections describe the characteristics of the model for two steady-state solutions: one in sliding (constant velocity) and one in presliding (zero velocity). The constant velocity behavior is similar to the behavior of the LuGre model. The presliding behavior is an improvement over the LuGre model due to the inclusion of a hysteresis model with nonlocal memory and the modeling of the hysteresis transition curves.

A. Constant Velocity Behavior

For constant velocity different from zero and in steady state ($dz/dt = 0$), (5) reduces to

$$\begin{aligned} \frac{dz}{dt} = 0 &= v\left(1 - \text{sign}\left(\frac{F_d(z)}{S(v) - F_b}\right) * \left|\frac{F_d(z)}{S(v) - F_b}\right|^n\right) \\ &\Downarrow \\ 1 &= \frac{F_d(z)}{S(v) - F_b} \\ &\Downarrow \\ S(v) &= F_d(z) + F_b. \end{aligned}$$

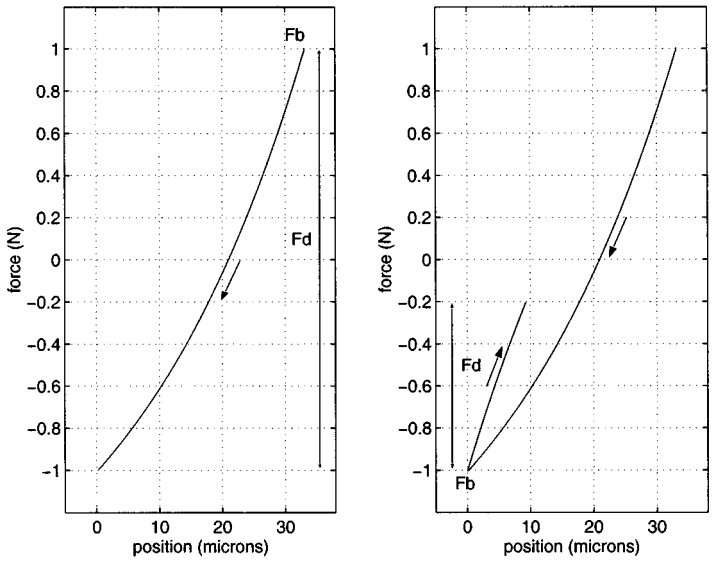

(a) (b)

Fig. 6. F_d and F_b before and after velocity reversal.

The friction force (3) reduces to

$$F = F_b + F_d(z) + \sigma_2 v$$
$$F = S(v) + \sigma_2 v. \tag{6}$$

The function $S(v)$ determines the constant velocity characteristics in the sliding regime near zero velocity while $\sigma_2 v$ becomes significant at high velocity. Choosing

$$S(v) = F_c + (F_s - F_c) * e^{-(v/v_s)^\delta} \tag{7}$$

with F_c the Coulomb friction, F_s the static friction, v_s the Stribeck velocity, and δ an arbitrary exponent, yields the classical Stribeck effect [7]. Extra flexibility can be built into (6) by assigning different values to F_s, F_c, v_s, δ, σ_2 for positive (F_s^+, F_c^+, v_s^+, δ^+, σ_2^+) and for negative (F_s^-, F_c^-, v_s^-, δ^-, σ_2^-) velocities, respectively.

B. Zero Velocity Behavior

For zero velocity, which corresponds to steady state in presliding, (3) and (5) reduce to

$$F = F_b + F_d(z) = F_h(z)$$
$$\frac{dz}{dt} = 0.$$

The hysteresis model relates the state variable z and the hysteresis force F_h. The implementation of the hysteresis model requires two memory stacks: one for the minima of F_h in ascending order (stack *m*) and one for the maxima of F_h (stack *M*). The stacks grow at a velocity reversal and shrink when an internal hysteresis loop is closed. The stacks are reset when the system goes from presliding to sliding. The value of F_b equals the most recent element of stack *M* if the transition curve is descending and of stack *m* if the transition curve is ascending. The value of the state variable z is reset to zero at each velocity reversal and recalculated at the closing of an internal loop.

The following three mechanisms govern the hysteresis model.

1) *Velocity reversal*: Velocity reversal results in a new extreme value for F_h which has to be added to one of the stacks: a maximum value for F_h is added to stack *M*, and a minimum value for F_h is added to stack *m*. After velocity reversal a new transition curve is started by setting F_b equal to F_h at the velocity reversal, i.e., the most recent element of the updated stack, and by resetting $F_d(z)$ and z to zero. Fig. 6 illustrates a reversal from a negative to a positive velocity and shows F_d and F_b before and after velocity reversal.
2) *Closing of an internal loop*: At the closing of an internal loop, the extreme values associated with this internal loop are removed from the stack. This is called the wiping out effect of hysteretic behavior [18]: if a hysteresis loop is closed, this loop is removed from the hysteresis memory, and the future hysteresis behaves as if this closed loop never occurred. Fig. 7 illustrates the closing of an internal loop by an ascending transition curve. $S_M(i)$ and $S_m(i)$ represent the values of stacks *M* and *m*, respectively. When the internal loop is closed, $S_M(i)$ and $S_m(i)$ are removed from these stacks, such that the $S_M(i-1)$ and $S_m(i-1)$ appear at the top of the stacks. The value of $S_m(i-1)$ becomes the F_b value for the ascending curve. The value of z is recalculated such that the new ascending curve continues the transition curve that started from $S_m(i-1)$ and ended at $S_M(i)$ (i.e., the beginning of the internal loop)

$$z = F_d^{-1}(S_M(i) - S_m(i-1)).$$

F_d^{-1} is the inverse function of the strictly increasing function F_d, i.e., $z = F_d^{-1}(F_d(z))$. This mechanism of the closing of an internal loop corresponds to the experimentally measured behavior as shown in Fig. 3.
3) *Resetting of the hysteresis model*: The hysteresis behavior disappears upon going from presliding to sliding. The

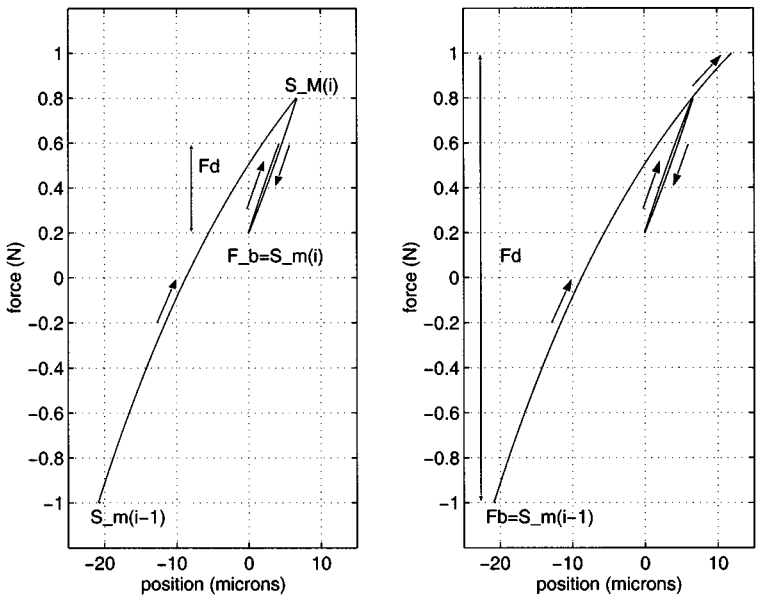

(a) (b)

Fig. 7. F_d and F_b before and after closing of internal loop.

hysteresis model is reset for strictly positive (respectively, strictly negative) velocities v when the hysteresis friction force $F_h(z)$ reaches a maximum (respectively, minimum) in presliding, i.e., when dz/dt becomes zero. This mechanism does not apply to extreme values of $F_h(z)$ reached at velocity reversals ($v = 0$) since then the system does not leave the presliding regime. Resetting of the hysteresis model corresponds to wiping out the hysteretic history, i.e., wiping out all the hysteresis transition curves which lie within the outermost hysteresis loop. The outermost hysteresis loop connects F_s^- to F_s^+. This is accomplished by resetting stack *m* to F_s^- and stack *M* to F_s^+. This corresponds to setting F_b equal to F_s^- (respectively, F_s^+) for positive (respectively, negative) velocities. At the same time, z is set to $F_d^{-1}(S(v)-F_s^-)$ $(F_d^{-1}(S(v)-F_s^+))$, so that the value of $F_h(z)$ remains unchanged. As a result, this resetting mechanism does not change dz/dt (=0) and the total friction force F [see (3) and (5)].

Remark 1: For certain transition curves $F_d(z)$ and for certain conditions of motion, transition from presliding to sliding shall occur only asymptotically, i.e., at infinite time. In other words, the hysteresis model will not be reset. Instead, the stacks will be cleaned up gradually by the mechanism of internal loop closing (the current transition curve forms a growing outer loop which gradually closes all smaller loops). This cleaning up will in the same way as the resetting mechanism eventually avoid possible overflow of the stack in practical implementations of the model. The predicted friction force will, however, be correct since both mechanisms influence the course of the state variable z and of the friction force in the same way.

Remark 2: The incorporation of this hysteresis function introduces extra model parameters which describe a single continuous transition curve (the outermost hysteresis loop which is assumed to correspond to the observed behavior). The number of parameters depends on how accurately one wishes to approximate measured transition curves as well as how complex those curves are. The practical example in Section IV-B describes that particular case by means of four turning points of a piece-wise linear curve, whereas the transition curves in [22] and [23] are described by means of a single continuous function depending on three parameters.

IV. Experimental Estimation of the Friction Model Parameters

This section describes the identification of the friction model parameters for the first joint of a KUKA IR 361 industrial robot. The axis of the first joint is vertical such that there is no gravity torque and the dynamics of the 1-DOF system can be described by the following equation:

$$I\frac{d^2x}{dt^2} = f - F. \tag{8}$$

Since this joint is rotational, I represents the mass moment of inertia of the robot about the first axis (all other robot axes are fixed), x is the angular position of the first joint, f is the driving torque, and F is the friction torque. The measurement of the motor current and the knowledge of the torque constant of the DC-motor yields the motor torque. The position is measured with an encoder mounted on the motor shaft. For more accurate position measurements an eddy-current proximity sensor installed on one of the transmission gears of the robot is used.

For the identification, the parameters of the model are divided into two groups: those which have mainly influence during the sliding regime and those which have mainly influence during the presliding regime.

A. Sliding

The parameter set for sliding regime depends on the choice of $S(v)$. The parameters are determined based on constant velocity tests over the full velocity range of the first joint. Fig. 8 shows

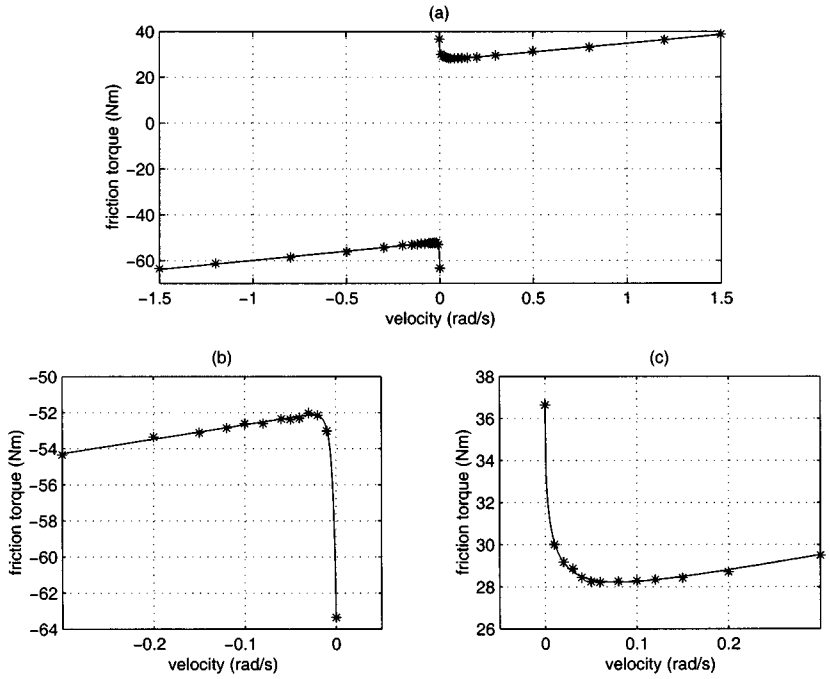

Fig. 8. Mean measured friction torques for different constant angular velocities (stars) and identified model $S(v)$ [see (7)] (solid line): (a) overall view and (b) and (c) details of left and right branch, respectively.

the mean measured friction for different constant positive and negative velocities. Table I shows the identified parameters for positive and negative velocities. The parameters are estimated using a Markov estimator [20], which is a weighted least squares estimator with the inverse of the sample variances of the torque measurements at the different velocities as the weights.

B. Presliding

The shape of the transition curve F_d and its parameters can be determined in a presliding experiment in which the applied force is slowly ramped up or down. Neglecting the dynamical effects, the viscous friction, and the micro-viscous damping, and considering that the applied force f is ramped up, (5) reduces to

$$\frac{dz}{dt} = v\left(1 - \left(\frac{f - F_b}{F_s^+ - F_b}\right)^n\right). \tag{9}$$

This equation allows calculating dz/dt for any preassumed value of n, and hence z since the latter is set to zero at velocity reversal. The value of $n = 7$ was chosen by *ad-hoc* optimization. It was found that the results are not very sensitive to the choice of n. Equation (9) also shows the implicit relationship between $z(dz/dt)$ and $x(v = dx/dt)$. The shape of the transition curve for the first joint of the KUKA 361 robot was, for simplicity, approximated by a piecewise linear function with four segments yielding eight parameters: in principle, the modeling of the transition curves can be carried out using any suitable approximation curve. Table II shows the estimated parameters (which are the coordinates of the turning points of the piecewise linear function) describing $F_d(z)$. These parameters were estimated only for a positive transition curve. The parameter values for negative transition curves are then set to the same values but with a negative sign, which should yield the same shape for positive as well as negative transition curves.

TABLE I
IDENTIFIED PARAMETERS WITH ESTIMATED VARIANCE FOR THE CONSTANT VELOCITY FRICTION FUNCTION $S(v)$ [see (7)]

parameter	positive velocity	negative velocity	units
F_s	36 ± 4	-63 ± 6	(Nm)
F_c	27 ± 1	-52 ± 1	(Nm)
v_s	0.007 ± 0.003	-0.004 ± 0.002	(rad/s)
δ	0.5 ± 0.2	0.9 ± 0.3	
σ_2	7.7 ± 0.2	8 ± 0.2	(Nms/rad)

TABLE II
ESTIMATED PARAMETERS FOR THE POSITIVE TRANSITION CURVE

position z (rad)	torque $F_d(z)$ (Nm)
0	0
$1.80e-06$	16.4
$1.41e-04$	75.1
$2.66e-04$	87.5
$5.21e-04$	100

The abscissas of the turning points (z) of the piecewise linear transition curves have, in this case, been arbitrarily chose. The ordinate values of the turning points F_d were, however, obtained via maximum likelihood estimation using two data sets: an averaged transition curve with the position measured by the standard encoder (Fig. 9) and a transition curve with more accurate position measurement using an eddy-current proximity sensor (Fig. 10). The proximity sensor signal was calibrated with the standard encoder signal taking into account a uniform probability distribution for the encoder measurements and a Gaussian distribution for the proximity sensor signal and minimizing the observable error between the two measurements. The resolution

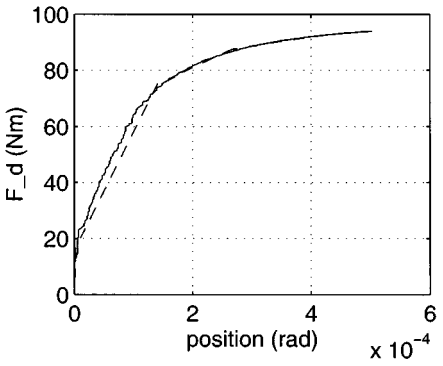

Fig. 9. Mean measured transition curve (solid line) and modeled transition curve F_d (dashed line) versus the robot joint angle x, for the first axis of the KUKA IR 361 robot using the motor encoder.

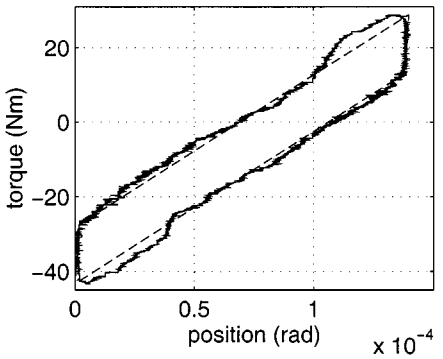

Fig. 10. Angular joint displacement-torque curve when ramping up and down the applied torque: measured with an eddy-current proximity sensor (solid line) and modeled (dashed line), for the first axis of the KUKA IR 361.

of the encoder and proximity sensor are $1.6\ 10^{-5}$ rad and $5\ 10^{-8}$ rad, respectively.

The use of a maximum likelihood estimator guarantees minimal parameter uncertainty and minimal sensitivity to noise since it takes the variance of the noise into account: noisy measurements have less impact on the parameter estimates than accurate measurements [20].

The influence of the parameter σ_1 was negligibly small to be observable on this test setup. However, a small positive value ($\sigma_1 = 1500$ Nms/rad, cf. an equivalent stiffness of about 9.110^6 Nm/rad and a velocity of the order of magnitude of 10^{-4} rad/s) had to be included to guarantee sufficient damping in the presliding regime. This measure was necessary in order to keep the simulation time step finite ($10^{-4}s$) and has no bearing on the overall model behavior.

V. Model Characteristics

This section shows that the presented model allows to predict dynamical characteristics such as stick-slip, varying break-away force, and frictional lag. Obviously these characteristics are similar to those of the LuGre model [9].

A. Stick-Slip Behavior

The model allows to simulate stick-slip behavior. Stick-slip motion can result when friction force decreases locally or globally with velocity. This usually takes place at low velocity and is accounted for by $S(v)$ [see (5)].

Stick-slip is observed on the first joint of the mentioned KUKA robot when this joint is controlled with a low gain proportional position feedback controller. Fig. 11 shows the simulated and the measured stick-slip behavior for a desired velocity of 0.1 rad/s and a proportional feedback gain of 1000 Nm/rad. The maximum relative error between the simulated and measured slip distances is 5.3%.

B. Varying Break-Away Torque and Time Lag

The model shows qualitatively the varying break-away torque and time lag behavior as described in the literature [3]. As the friction torque is not measured directly, the KUKA 361 IR test setup, which corresponds to industrial needs, does not allow to measure directly this dynamical behavior of the friction. This would only possible in specially designed friction test setups.

When the driving torque is ramped up with a constant rate, the friction torque opposing the driving torque also increases as long as the system sticks. When the system breaks away and starts to slide, the friction torque reaches a maximum since the friction torque decreases with velocity in the low velocity sliding regime due to the Stribeck-effect (Fig. 12). The maximum friction torque is larger for smaller rates and smaller for larger rates. Fig. 13 shows the maximum friction torque, resulting from the identified model, as a function of the rate with which the applied torques is ramped up from zero. The results are qualitatively in correspondence with the results described in the literature.

When sinusoidally ramping up and down the velocity in the Stribeck velocity region, the relation between friction and velocity is hysteretic (Fig. 14). The friction torque is smaller for decreasing velocities than for increasing velocities. The breadth of the hysteresis loop increases with the rate of the velocity changes. This behavior corresponds to a time delay between velocity and friction force.

VI. Applications

This section describes two applications of the developed friction model: the prediction of the presliding friction force on a linear slideway and the accurate tracking at very low velocities for the first joint of the KUKA 361 IR robot.

A. Presliding Friction Modeling for a Linear Slideway

Machine tools are an important class of machines for which positioning accuracy directly influences product quality. Typical positioning systems, e.g., an X–Y table, contain linear slideways. Rolling element slideways can be designed such that the Stribeck effect is virtually absent, but they will still exhibit a nonlinear presliding friction behavior which introduces machining errors such as quadrant glitches [24]. Friction modeling and model-based friction compensation, as described in [21] and [22] for rolling element slideways, are required to reduce these errors.

Reference [21] describes presliding friction modeling for linear slideways. It corresponds to the modeling of the transition curves F_d based on very accurate position, acceleration, and force measurements. Fig. 15 shows the measured and the

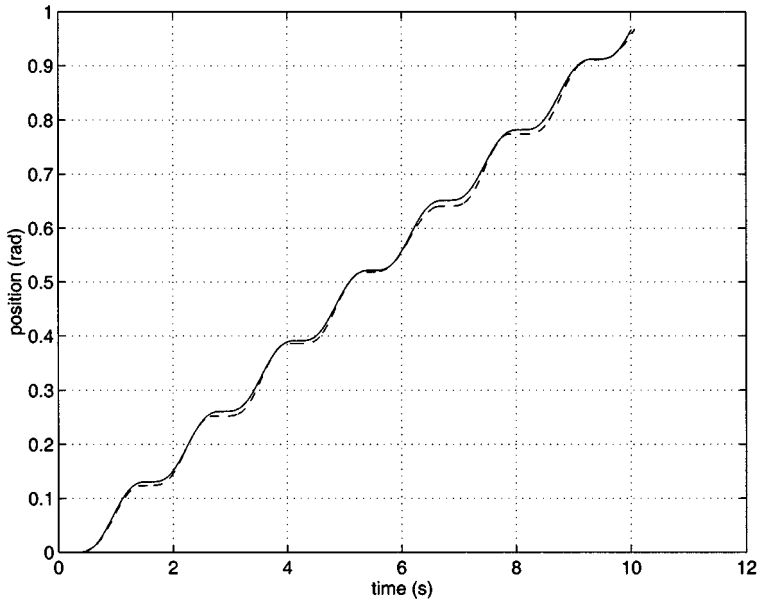

Fig. 11. Stick-slip behavior predicted by the model (solid line) and measured on the first axis of the KUKA IR 361 robot (dashed line).

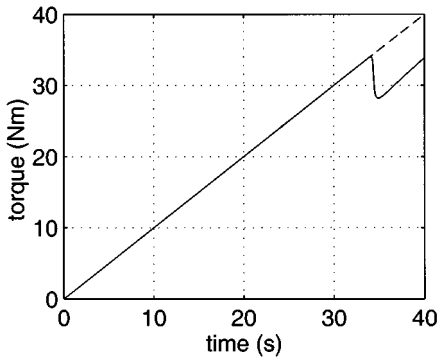

Fig. 12. Experimental results obtained on the first axis of the KUKA IR 361 robot, when the applied torque is ramped up with constant rate: applied torque (dashed line) and measured friction torque (solid line).

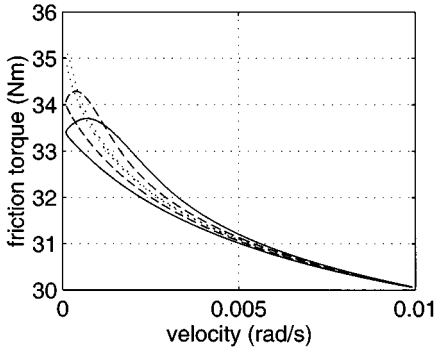

Fig. 14. Stribeck friction torque for sinusoidally varying velocity at different frequencies f_v: $f_v = 0.25$ Hz (solid line), $f_v = 0.1$ Hz (dashed line), and $f_v = 0.01$ Hz (dotted line).

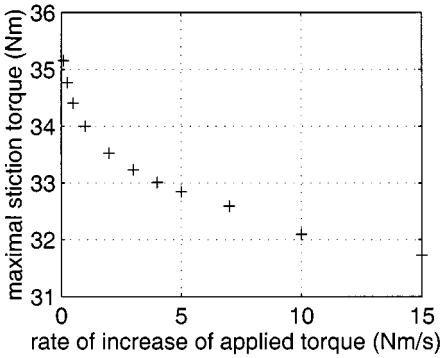

Fig. 13. Varying break-away torque for different rates of increase of applied torque.

modeled presliding friction force. The measurement clearly shows a hysteretic behavior with nonlocal memory. The model parameters of $F_d(z)$ are identified for the outer hysteresis transition curves only, yet the correspondence between prediction and measurement is excellent.

B. Accurate Tracking at Very Low Velocities

Accurate tracking at extremely low velocities requires accurate knowledge of friction. Schemes that achieve this accurate tracking at low velocities can be divided in two groups.

- Schemes that do not need a friction model for compensation. These schemes measure directly the inertial forces or the friction force. References [19] and [16] present a precise robot control approach based on base wrench measurements. This method does not require friction modeling but requires the mounting of the robot on an expensive force-torque sensor.
- Schemes that use a friction model to compensate for the friction force. These schemes need less sensors and data acquisition, yet they require an accurate friction model and computing time to evaluate the friction model. Reference [17] presents a feedforward friction compensation method for an X–Y table based on an experimentally optimized (using accelerated evolutionary programming) classical friction model described in [3].

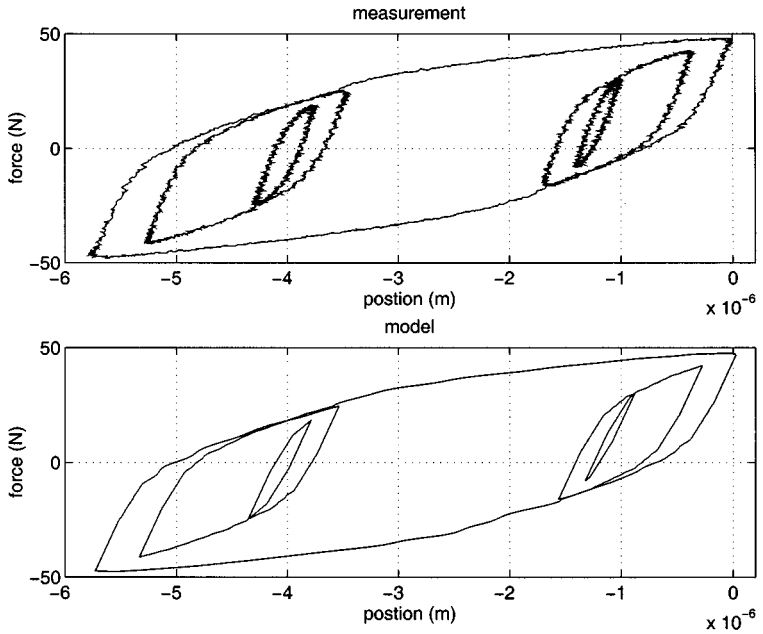

Fig. 15. Measured and modeled presliding friction force for a linear slideway.

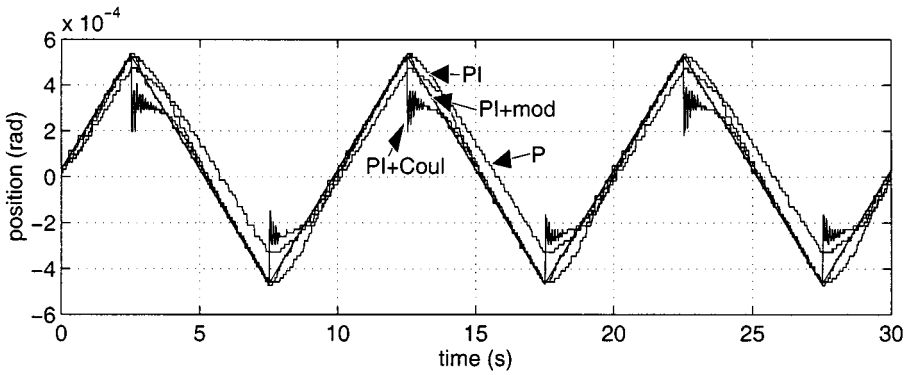

Fig. 16. Desired position and measured position for four different controllers; PI+Coul indicates PI-control plus Coulomb friction compensation; and PI+mod indicates PI-control plus full friction model compensation.

This section shows the result of a feedforward friction compensation approach based on the identified model for the first axis of the KUKA IR 361 robot. The model-based feedforward control shows an improved tracking performance in comparison with pure feedback or feedforward friction compensation based on a Coulomb friction model.

The desired trajectory is a triangular waveform. The positions have been measured with the standard encoder mounted on the rotor, one encoder step corresponds to 1.63 10^{-5} rad at the link side. The period is 10 s and the velocity is 2 10^{-4} rad/s corresponding to 12.275 encoder steps/s. Four controllers are compared: a proportional controller, a Proportional+Integral controller, a PI-controller with feedforward based on a Coulomb friction model, and a PI-controller with feedforward based on the identified friction model. The Coulomb friction compensation uses the identified values F_c of Table I. During the motion, the robot moves through the presliding and sliding regimes. Fig. 16 shows the desired trajectory and the measured trajectories for the different controllers. Fig. 17 shows the tracking errors for the different controllers.

Table III shows the root mean square tracking error and the maximum tracking error for the four control laws. The PI-controller with feedforward of the Coulomb friction torque is not better than the PI-controller for this low velocity tracking:

- The friction behaves as a flexible system (nonlinear spring) in the presliding regime. After a velocity reversal, only a small fraction of the predicted Coulomb friction torque is needed to obtain small displacements, i.e., feedforward of the full Coulomb friction torque results in overcompensation thus yielding large tracking errors. Once the actual friction torque becomes larger than the predicted Coulomb friction, the tracking errors with Coulomb friction feedforward become smaller than in the case when feedforward is not present. A feedforward of the Coulomb friction will also yield better tracking results in the sliding regime than pure feedback control.
- The proportional and integral controller constants are very high, i.e., 80% of the values that make the system unstable.

Addition of the full model-based friction feedforward to the PI-control reduces the maximum tracking error by a factor of

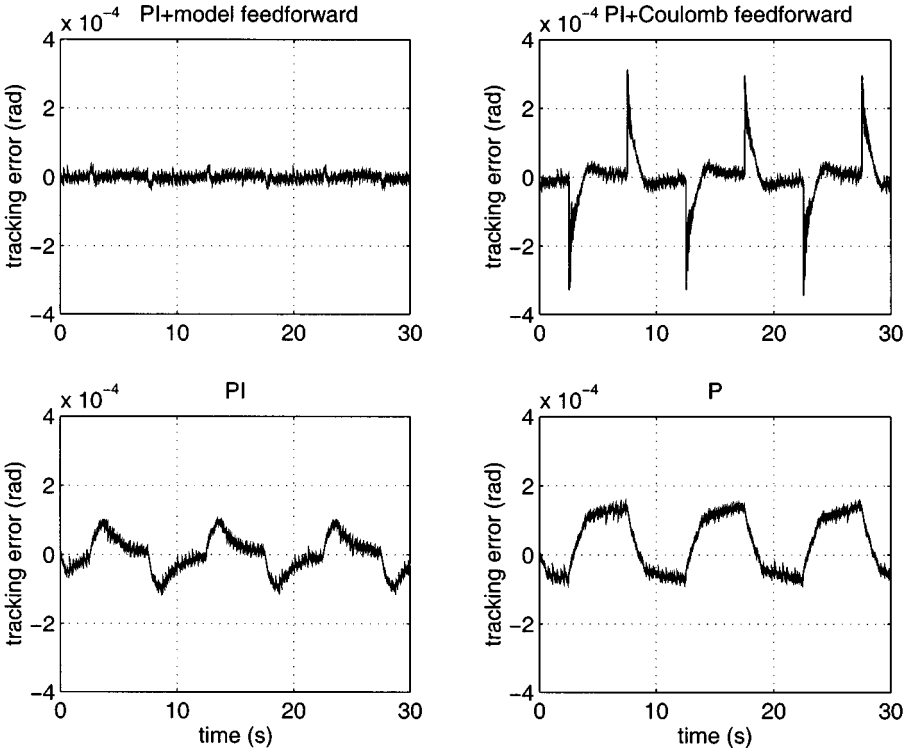

Fig. 17. Tracking errors for the four controllers.

TABLE III
TRACKING ERRORS FOR THE FOUR CONTROLLERS

	$\sqrt{(mean(error^2))}$	max. error
PI+model feedforward	$9.4\ 10^{-06}$	$3.3\ 10^{-05}$
PI+Coulomb feedforward	$6.1\ 10^{-05}$	$3.5\ 10^{-04}$
PI	$4.9\ 10^{-05}$	$1.1\ 10^{-04}$
P	$8.7\ 10^{-05}$	$1.5\ 10^{-04}$

3.25 and the root mean square error by a factor of 5.26, yielding a maximum tracking error which is less than two encoder steps and a root mean square tracking error of 57% of an encoder step.

Remark: Dependence of the friction force on the position, normal force, and temperature can be taken into account using a scaling function or factor in the friction force (3) or in the nonlinear state equation (5), [13], [8], [3]. Canudas de Wit *et al.* [8] describe, for the LuGre model, the on-line estimation of a scaling factor accounting for normal load and temperature variations in an adaptive friction compensation approach. Ganseman [13] describes, for the model described in this paper, an off-line identified scaling function accounting for the position and normal load dependence of the friction force.

VII. CONCLUSION

This paper presents a dynamical friction model which is valid in both the sliding and the presliding regimes. Presliding friction is modeled by means of an hysteresis model with nonlocal memory.

The model can account accurately for experimentally obtained friction characteristics: Stribeck friction in sliding, hysteretic behavior in presliding, frictional lag, varying break-away, and stick-slip behavior, as has been demonstrated by a series of experimental tests.

It can be concluded that the developed dynamical friction model can accurately describe any friction behavior as observed in experiments or described in the literature. The flexibility in the parameterization allows a good fitting of experimentally obtained results. In this way, the developed model is one of the most effective friction models for description of experimentally observed friction behavior. Being flexible, the obtained model structure is also capable of further extension and generalization to include other effects such as position dependence of friction behavior and possible cyclic softening (or hardening) of the hysteresis "spring" characteristic. This will be the subject of future work that will also include application of the model in friction compensation of robots and machine tools.

ACKNOWLEDGMENT

This text presents research results of the Belgian programme on Interuniversity Poles of attraction initiated by the Belgian State, Prime Minister's Office, Science Policy Programming. The scientific responsibility is assumed by its authors.

REFERENCES

[1] F. Altpeter, P. Myszkorowski, M. Kocher, and R. Longchamp, "Friction compensation: Pid synthesis and state control," in *European Control Conf. ECC*, Brussels, Belgium, 1997, TH-M-I1.

[2] B. Armstrong, "Challenges to systematically engineered friction compensation," in *Proc. IFAC Workshop Motion Control*, Munich, Germany, Oct. 9, 1995, pp. 21–30.

[3] B. Armstrong-Hélouvry, *Control of Machines with Friction*. New York: Kluwer, 1991.

[4] B. Armstrong-Hélouvry, P. Dupont, and C. Canudas de Wit, "A survey of models, analysis tools and compensation methods for the control of machines with friction," *Automatica*, vol. 30, no. 7, pp. 1083–1138, 1994.
[5] R. Arnell, P. Davies, J. Halling, and T. Whomes, *Tribology*. London, U.K.: Macmillan, 1991.
[6] S. Björklund, "A random model for micro-slip between nominally flat surfaces," *ASME J. Tribology*, vol. 119, pp. 726–732, 1997.
[7] L. Bo, "The friction-speed relation and its influence on the critical velocity of stick-slip motion," *Wear*, vol. 82, no. 3, pp. 277–289, 1982.
[8] C. Canudas de Wit and P. Lischinsky, "Adaptive friction compensation with partially known dynamic friction model," *Int. J. Adaptive Control Signal Processing*, vol. 11, pp. 65–80, 1997.
[9] C. Canudas de Wit, H. Olsson, K. Aström, and P. Lischinsky, "A new model for control of systems with friction," *IEEE Trans. Automat. Contr.*, vol. 40, pp. 419–425, May 1995.
[10] P. R. Dahl, "A solid friction model," The Aerospace Corporation, El Segundo, CA, Tech. Rep. TOR-158(3107-18), 1968.
[11] B. Eriksson, "Optimal force control to improve hydraulic drives," Ph.D. dissertation, Department of Machine Design, Royal Institute of Technology, KTH, DAMEK Research Group, Stockholm, Sweden, 1996.
[12] S. Futami, A. Furutani, and S. Yoshida, "Nanometer positioning and its micro-dynamics," *Nanotechnology*, vol. 1, no. 1, pp. 31–37, 1990.
[13] C. Ganseman, "Dynamic modeling and identification of mechanisms with application to industrial robots," Ph.D. dissertation, Division PMA, Dept. of Mechanical Engineering, K.U. Leuven, Leuven, Belgium, 1998.
[14] C. Ganseman, J. Swevers, T. Prajogo, and F. Al-Bender, "An integrated friction model with improved presliding behavior," in *Proc. Symp. Robot Control*, Nantes, France, 1997, pp. 221–226.
[15] D. Hess and A. Soom, "Friction at a lubricated line contact operating at oscilating sliding velocities," *ASME J. Tribology*, vol. 112, no. 1, pp. 147–152, 1990.
[16] K. Iagnemma, G. Morel, and S. Dubowsky, "A model-free fine position control method using the base-sensor: With application to a hydraulic manipulator," in *Symp. Robot Control*, Nantes, France, 1997.
[17] J.-H. Kim, H.-K. Chae, J.-Y. Jeon, and S.-W. Lee, "Identification and control of systems with friction using accelerated evolutionary programming," *IEEE Contr. Systems*, pp. 38–47, Aug. 1996.
[18] I. D. Mayergoyz, *Mathematical Models of Hysteresis*. New York: Springer-Verlag, 1991.
[19] G. Morel and S. Dubowsky, "The precise control of manipulators with joint friction: A base force/torque sensor method," in *Proc. IEEE Int. Conf. Robotics and Automation*, Minneapolis, MN, 1996, pp. 360–365.
[20] J. P. Norton, *An Introduction to Identification*. London, U.K.: Academic, 1986.
[21] T. Prajogo, F. Al-Bender, and H. Van Brussel, "Study of the friction behavior of rolling element slideways," in *Proc. Pacific Conf. Manufacturing*, Jakarta, Indonesia, 1994, pp. 508–516.
[22] ——, "Identification of pre-rolling friction dynamics of rolling element bearings: Modeling and application to precise positioning systems," in *Proc. 8th Int. Precision Engineering Seminar*, Compiègne, France, 1995, pp. 229–232.
[23] P. F. Rogers and G. Boothroyd, "Damping at metallic interfaces subjected to oscillating tangential loads," *ASME J. Engineering for Industry*, pp. 1087–1093, 1975.
[24] E. Tung, G. Anwar, and M. Tomizuka, "Low velocity friction compensation and feedforward solution based on repetitive control," *Trans. ASME, J. Dynamic Syst., Measurement, and Contr.*, vol. 115, pp. 279–284, June 1993.

Jan Swevers was born in Leuven, Belgium, in 1963. He received the B.E. degree in electrical engineering in 1986, from the Katholieke Universiteit Leuven, Belgium, and joined its Department of Mechanical Engineering, Division P.M.A. (production, machine design, and automation) in the same year, where he received the Ph.D. degree in mechanical engineering in 1992. He continued working at the same division as a Senior Research Assistant for the Fund for Scientific Research, Flanders. During 1997, he was a Postdoctoral Researcher of the Katholieke Universiteit Leuven.

He became an Assistant Professor in 1995. His research interests include various aspects of system identification and control.

Farid Al-Bender received the B.Eng. (Hon.) degree in mechanical engineering from the University of Sheffield, U.K., in 1975, and the M.Sc. degree in tribology from the University of Leeds, U.K., in 1976.

Having worked as a Maintainance Engineer and as an Assistant Lecturer in mathematics (University of Constantine, Algeria, 1980–1985), he joined the K.U. Leuven, Department of Mechanical Engineering, as a Research Assistant in 1985, in the framework of a research program on aerostatic bearings leading to the Ph.D. degree, in 1992. Since then, he has been a Senior Research Associate there, Lecturer in tribology and co-lecturing in precision mechanics. His main research interests include the design and development of air bearing and precision systems, active control of aerostatic bearings, and engineering tribology.

Chris G. Ganseman received the Master's degree in 1992 and the Ph.D. degree in 1998, both in mechanical engineering from the Katholieke Universiteit Leuven, Belgium.

From 1993 to 1997, he was a Research Assistant at the Katholieke Universiteit Leuven in the field of automation and robotics with emphasis on the modeling and experimental identification of the dynamical behavior of mechanisms and robots. In 1997, he joined New Holland and worked in the service and quality departments before joining the Combine Engineering Department. His main activities include cab design, sensor development and automation, and engineering methods and standards.

Tutuko Prajogo received the Mechanical Engineering degree from Institut Teknologi Bandung (ITB), Indonesia, in 1987.

He joined Indonesian's Nusantara Aircraft Industry and BPPT's MEPPO Laboratory in 1988. He received the M.S. in manufacturing engineering from the University of Southern California, USA, in 1991 and continued working for the MEPPO Laboratory. He is currently involved in the research of friction identification, modeling and compensation in the machine tool area at the PMA Division, Department of Mechanical Engineering, Katholieke Universiteit Leuven, Belgium.